Anaplerotic flux into the Calvin-Benson cycle. Integration in carbon and energy metabolism of *Helianthus annuus*

Thomas Wieloch[a,*], Angela Augusti[b], Jürgen Schleucher[a]

Author affiliations

[a] Department of Medical Biochemistry and Biophysics, Umeå University, 901 87 Umeå, Sweden

[b] Research Institute on Terrestrial Ecosystems, National Research Council, 05010 Porano (TR), Italy.

* To whom correspondence may be addressed.

email: thomas.wieloch@umu.se

phone: +46706460369

Author	Email address	ORCID
Thomas Wieloch	thomas.wieloch@umu.se	0000-0001-9162-2291
Angela Augusti	angela.augusti@cnr.it	0000-0002-9591-693X
Jürgen Schleucher	jurgen.schleucher@umu.se	

Abstract

Plants assimilate carbon primarily via the Calvin-Benson cycle. Two companion papers reports evidence for anaplerotic carbon flux into this cycle. To estimate flux rates in *Helianthus annuus* leaves based on gas exchange measurements, we here expanded Farquhar-von Caemmerer-Berry photosynthesis models by terms accounting for anaplerotic respiration and energy recycling. In line with reported isotope evidence (companion papers), we found relative increases in anaplerotic flux as intercellular CO_2 concentrations, C_i, decrease below a change point. At C_i=136 and 202 ppm, we found absolute rates of 2.99 and 2.39 µmol Ru5P m^{-2} s^{-1} corresponding to 58.3 and 28.2% of net CO_2 assimilation, 13.1 and 10.7% of ribulose 1,5-bisphosphate regeneration, and 22.2 and 15.8% of Rubisco carboxylation (futile carbon cycling), respectively. Anaplerotic respiration governs total day respiration with contributions of 81.3 and 77.6%, and anaplerotic relative to photorespiratory CO_2 release amounts to 63.9 and 67%, respectively. Furthermore, anaplerotic flux significantly increases absolute ATP demands and ATP-to-NADPH demand ratios of photosynthesis and may explain increasing sucrose-to-starch carbon partitioning ratios with decreasing C_i. We propose that anaplerotic flux can occur under both Rubisco and RuBP-limited growth conditions. Overall, our work introduces the anaplerotic pathway as central component in carbon and energy metabolism of C_3 plants.

Keywords: Calvin-Benson cycle; oxidative pentose phosphate pathway; glucose-6-phosphate shunt; Farquhar-von Caemmerer-Berry photosynthesis model; net CO_2 assimilation; day respiration; ATP-to-NADPH ratio; sucrose-to-starch carbon partitioning

This manuscript has two companion papers:

(1) **Wieloch T, Grabner M, Augusti A, Serk H, Ehlers I, Yu J, Schleucher J**. 2021. Metabolism is the major driver of hydrogen isotope fractionation recorded in tree-ring glucose of *Pinus nigra*. bioRxiv.

(2) **Wieloch T, Augusti A, Schleucher J.** 2021. Anaplerotic flux into the Calvin-Benson cycle. Isotope evidence for *in vivo* occurrence in *Helianthus annuus*. bioRxiv.

Introduction

Anaplerotic carbon flux into the Calvin-Benson cycle (CBC) may occur via two metabolic routes (Fig. 1). The first was proposed by Eicks et al. (2002) reporting the discovery of the xylulose 5-phosphate/phosphate translocator in *Arabidopsis thaliana*. This transporter enables exchange of pentose phosphates, and inorganic phosphate across chloroplast envelops. Screening *Arabidopsis* genome databases, these authors found genes encoding for (i) the complete chloroplastic pentose phosphate pathway, (ii) the oxidative branch of the cytosolic pentose phosphate pathway, and (iii) cytosolic ribulose-5-phosphate epimerase and ribose-5-phosphate isomerase. Genes encoding for cytosolic transketolase and transaldolase required to process pentose phosphates were missing. Because of the concomitant lack of fate for pentose phosphates in the cytosol, Eicks et al. (2002) proposed their translocation into chloroplasts and injection into the CBC. Recently, Sharkey et al. (2020) proposed that cytosolic carbon re-entering chloroplasts by this route may explain the temporal lag in ^{13}C labelling of CBC pools in plants fed $^{13}CO_2$. The second route, proposed by Sharkey and Weise (2016), involves glucose 6-phosphate (G6P) to ribulose 5-phosphate (Ru5P) conversion via the oxidative branch of the pentose phosphate pathway inside chloroplasts and injection of Ru5P into the CBC. Wieloch et al. (2018) and the companion papers report evidence supporting flux through this route. These authors explain increasing metabolic deuterium fractionation, ε_{met}, at HC-1 of leaf starch in *Helianthus annuus* and *Pinus nigra* with relative increases in anaplerotic flux inside chloroplasts. Increases occur as intercellular CO_2 concentrations, C_i, decrease below a change point (Fig. 2a, blue squares).

For each molecule Ru5P synthesised by anaplerotic pathways, one molecule CO_2 is liberated from metabolism while two molecules NADPH are recycled (Fig. 1). These effects can be expected to impact on overall photosynthesis, plant performance, growth, and biosphere-atmosphere CO_2 exchange. Hence, it is central to determine whether and when flux through anaplerotic pathways occurs at what rate. Since anaplerotic flux involves CO_2 liberation, it can be expected to have effects on leaf gas exchange which may be traceable by modelling gas exchange data. To test this, (i) we expand Farquhar-von Caemmerer-Berry (FvCB) photosynthesis models by terms accounting for anaplerotic respiration and energy recycling, and (ii) estimate anaplerotic flux rates and associated effects on leaf carbon and energy metabolism. Gas exchange data reported here and ε_{met} data in companion paper 2 were collected during the same experiment from the same *Helianthus annuus* plants.

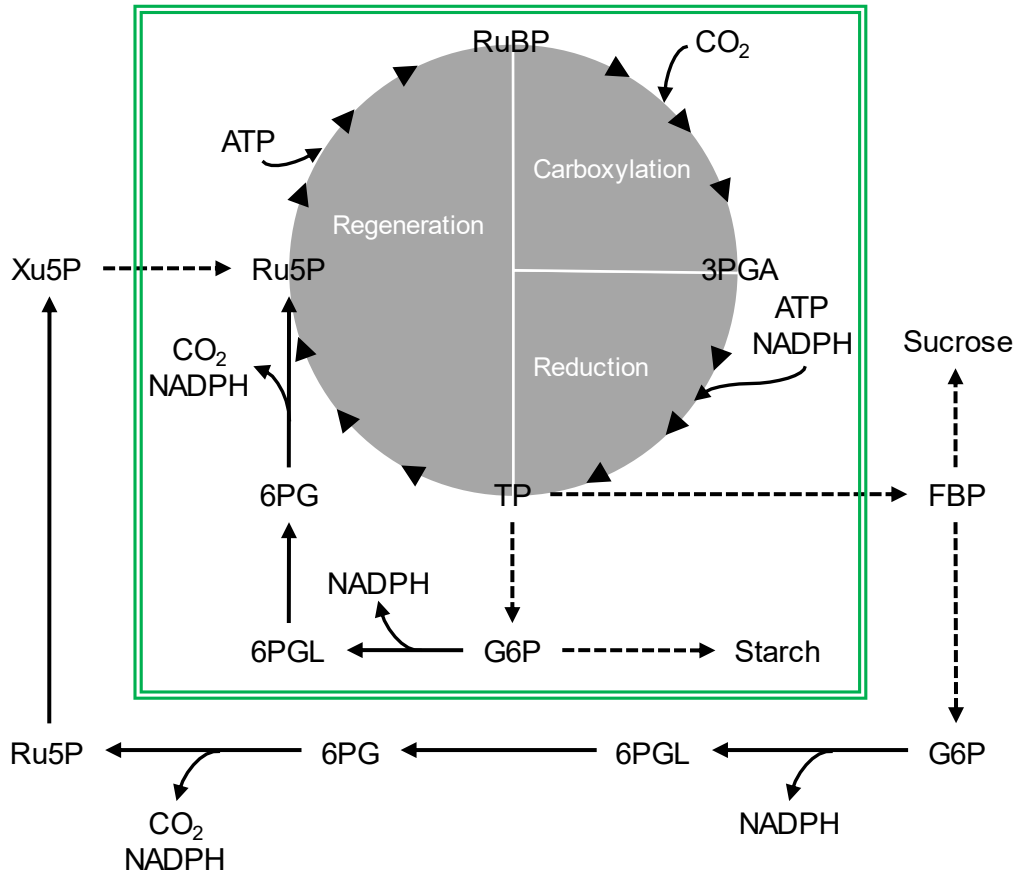

Figure 1 Anaplerotic carbon flux into the Calvin-Benson cycle and sucrose-to-starch carbon partitioning. Metabolites: 3PGA, 3-phosphoglycerate; 6PG, 6-phosphogluconate; 6PGL, 6-phosphogluconolactone; ATP, adenosine triphosphate; F6P, fructose 6-phosphate; FBP, fructose 1,6-bisphosphate; G6P, glucose 6-phosphate; NADPH, nicotinamide adenine dinucleotide phosphate; Ru5P, ribulose 5-phosphate; RuBP, ribulose 1,5-bisphosphate; TP, triose phosphates (glyceraldehyde 3-phosphate, dihydroxyacetone phosphate); Xu5P, Xylulose 5-phosphate. Chloroplast and cytosolic metabolism inside and outside the green box, respectively. Solid and dashed arrows represent transformations catalysed by a single enzyme or multiple enzymes, respectively.

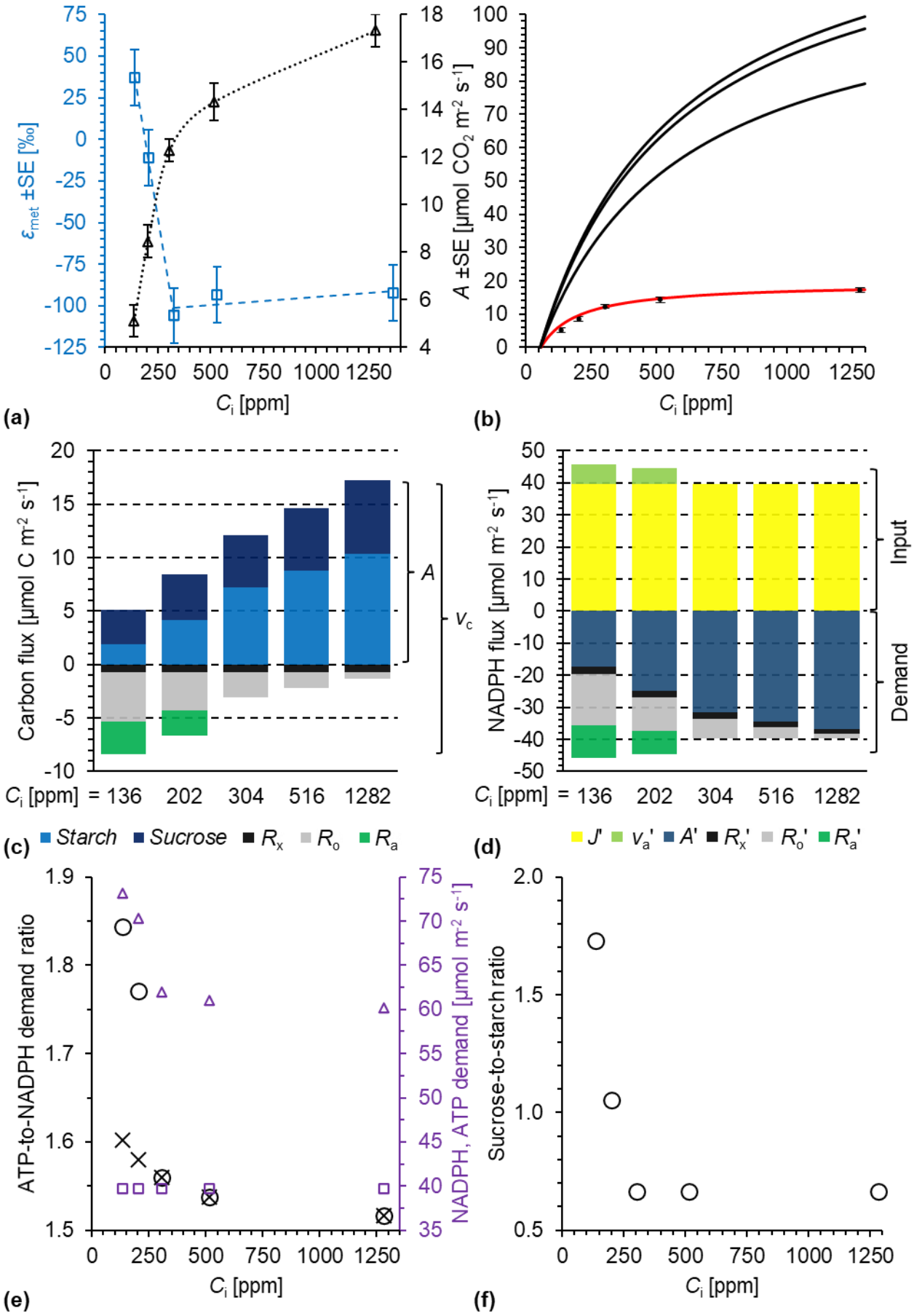
(a)
ε_{met} ±SE [‰]
A ±SE [µmol CO2 m-2 s-1]
Ci [ppm]
(b)
Ci [ppm]
(c)
Carbon flux [µmol C m-2 s-1]
A
vc
Ci [ppm] = 136 202 304 516 1282
Starch Sucrose Rx Ro Ra
(d)
NADPH flux [µmol m-2 s-1]
Input
Demand
Ci [ppm] = 136 202 304 516 1282
J' va' A' Rx' Ro' Ra'
(e)
ATP-to-NADPH demand ratio
NADPH, ATP demand [µmol m-2 s-1]
Ci [ppm]
(f)
Sucrose-to-starch ratio
Ci [ppm]

88

Figure 2 (a) Metabolic D fractionation, ε_{met}, at starch HC-1 (blue squares, companion paper 2) and net CO_2 assimilation, A, of *Helianthus annuus* leaves (black triangles). Plants were grown in a greenhouse at C_a=450 ppm and then moved to growth chambers. After a day in darkness to drain starch reserves, plants were grown at different levels of C_a (180, 280, 450, 700, 1500 ppm) corresponding to different levels of C_i (140, 206, 328, 531, and 1365 ppm) for two days. During gas exchange measurements slightly lower C_i levels prevailed (136, 202, 304, 516, 1282 ppm). ε_{met} was calculated as $\varepsilon_{met}=D_1/1/5\Sigma(D_3, D_4, D_5, D_{6S}, D_{6R})-1)*10^3$ with D_i denoting deuterium abundances at intramolecular HC-*i* positions of glucose (±SE=16.7‰, n≥3). Figure shows discrete data. Dashed and dotted lines added to guide the eye. **(b)** Net CO_2 assimilation of *Helianthus annuus* leaves as function of C_i. Black dots with standard error intervals, measured values (±SE=0.65 µmol CO_2 m^{-2} s^{-1}, n=8); red line, modelled RuBP-limited assimilation, A_j; black lines, Rubisco-limited assimilation modelled with different literature-derived values for V_{cmax} (≈112, ≈135, and ≈140 µmol m^{-2} s^{-1}) (Wullschleger, 1993; Walker *et al.*, 2014; Kattge *et al.*, 2020). **(c)** Carbon balance of *Helianthus annuus* leaves. Flux estimates come from a model of RuBP-limited net CO_2 assimilation which considers respiration and energy recycling by the anaplerotic pathway. R_o, photorespiratory CO_2 release (R_o=0.5v_o); R_a, anaplerotic respiration; R_x, respiration by other processes. **(d)** Energy (NADPH) balance of *Helianthus annuus* leaves. J', NADPH input via whole chain electron transport (2J); v_a', NADPH input by the anaplerotic pathway (2v_a); A', NADPH demand by net CO_2 assimilation (-(2+4Γ_*/C_c)A); R_o', R_a', and R_x', NADPH demands for net assimilation of CO_2 released by photorespiration, anaplerotic respiration, and other respiratory processes, respectively (-(2+4Γ_*/C_c) $R_{o,\ a,\ or\ x}$). **(e)** Demand for energy and reducing equivalents by CO_2 assimilation in *Helianthus annuus* leaves. Purple triangles, ATP demand ((3+7Γ_*/C_c)v_c); purple squares, NADPH demand ((2+4Γ_*/C_c)v_c-2v_a); black circles, ATP-to-NADPH demand ratio considering anaplerotic NADPH recovery; black crosses, ATP-to-NADPH demand ratio neglecting anaplerotic NADPH recovery. **(f)** Modelled sucrose-to-starch carbon partitioning ratio in *Helianthus annuus* leaves. Rubisco carboxylation rate, v_c, equals the sum over all absolute individual fluxes in figure 2c. To estimate fluxes into sucrose and starch, a carbon fraction given by v_c-R_o-R_x was assumed to be allocated into the sucrose and starch biosynthesis pathways at a constant 2:3 ratio (Sharkey *et al.*, 1985) with the anaplerotic flux diverting a carbon fraction v_a from the starch biosynthesis pathway into the CBC.

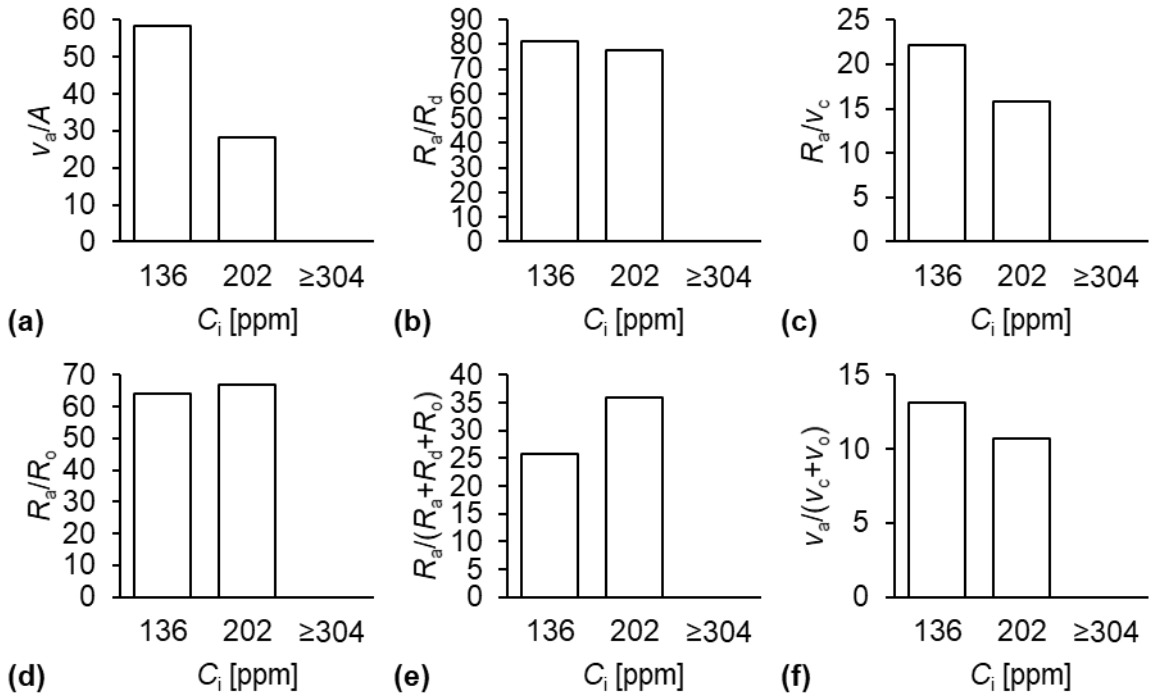

Figure 3 Flux ratios at different intercellular CO_2 concentrations in percent. **(a)** Anaplerotic flux relative to net CO_2 assimilation. **(b)** Contribution of anaplerotic respiration to day respiration. **(c)** Futile carbon cycling involving Rubisco carboxylation and anaplerotic respiration. **(d)** Anaplerotic respiration relative to photorespiratory CO_2 release. **(e)** Anaplerotic relative to total CO_2 release. **(f)** Anaplerotic contribution to ribulose 1,5-bisphosphate regeneration. Symbols: anaplerotic flux in terms of ribulose 5-phosphate, v_a; anaplerotic respiration, R_a; CO_2 liberation by processes other than photorespiration or the anaplerotic pathway in chloroplasts, R_x; day respiration, R_d; intercellular CO_2 concentration, C_i; net CO_2 assimilation, A; photorespiratory CO_2 release, R_o; Rubisco carboxylation, v_c; Rubisco oxygenation, v_o. Measurements and estimates come from gas exchange experiments and modelling on *Helianthus annuus* leaves. Plants were grown in a greenhouse at C_a=450 ppm and then moved to growth chambers. After a day in darkness to drain starch reserves, plants were grown at different levels of C_a (180, 280, 450, 700, 1500 ppm) corresponding to different levels of C_i (140, 206, 328, 531, and 1365 ppm) for two days. During gas exchange measurements slightly lower C_i levels prevailed (136, 202, 304, 516, 1282 ppm).

Results

Phases in the A/C_i curve

It is generally believed that A/C_i curves enable identification of metabolic processes limiting CO_2 assimilation (A denotes net CO_2 assimilation) (Farquhar *et al.*, 1980). Initial linear increases in these curves are commonly attributed to Rubisco-limited assimilation, A_c (Fig. 2a,

dotted black line). A change point in the response of A to C_i, also known as deflection point, DP, marks the onset of RuBP-limited assimilation, A_j. RuBP limitation is attributed to limitations in energy supply. At high C_i and high light, assimilation can be limited by triose phosphate utilisation (Sharkey, 1985). However, plants studied here were grown at low light (300 to 400 µmol photons m^{-2} s^{-1}). Thus, limitation by triose phosphate utilisation is unlikely. While the resolution of our A/C_i data is low, two phases can be clearly distinguished (Fig. 2a, black dotted line). A change point at $C_i \approx 300$ ppm separates the initial linear increase from RuBP-limited assimilation. According to ε_{met} measurements (Fig. 2a, dashed blue line), upregulated anaplerotic flux overlaps with the initial linear increase of CO_2 assimilation. The deflection point closely overlaps with the C_i change point where anaplerotic flux is downregulated. Constantly downregulated anaplerotic flux overlaps with RuBP-limited assimilation.

Metabolic mechanisms regulate anaplerotic flux

Leaf starch used for ε_{met} measurements was synthesised in a stable environment where only C_a was varied (Fig. 2a). Net CO_2 assimilation rates increased over the entire C_a range showing that carbon metabolism was sensitive to all C_a levels applied (up to C_a=1431 ppm, C_i=1282 ppm). By contrast, anaplerotic flux into the CBC was insensitive to C_a changes above 450 ppm (C_i=328 ppm). Thus, the change point in ε_{met} reflects a change point in metabolism, not in the environment. That is, above DP, anaplerotic flux is deactivated or maintained at constant relative levels by metabolic mechanisms.

Estimating day respiration

Under standard conditions (400 ppm CO_2, 21% O_2, 20-25 °C), day respiration, R_d, commonly is a 5% fraction of net CO_2 assimilation attributed to CO_2 liberation by the pyruvate dehydrogenase complex, cytosolic glucose-6-phosphate dehydrogenase, isocitrate dehydrogenase, and the α-ketoglutarate dehydrogenase complex (Atkin *et al.*, 2000; Teskey *et al.*, 2017). Here, we assume that absolute rates of CO_2 liberation by these enzymes are constant over the entire C_a range. This includes the anaplerotic pathway described by Eicks et al. (2002) which starts at cytosolic glucose-6-phosphate dehydrogenase. By contrast, anaplerotic flux in chloroplasts and associated respiration evidently varies below the deflection point of the A/C_i curve (Fig. 2a, companion paper 2). Hence, we partition R_d into a variable component reflecting chloroplastic anaplerotic respiration, R_a, and a constant component reflecting respiration by other pathways, R_x, as

$$R_{\mathrm{d}} = R_{\mathrm{a}}\mathrm{I}(C_{\mathrm{i}} < DP) + R_{\mathrm{x}} \qquad \text{[Eq. 1]}$$

where DP is the C_i value at the deflection point of the A/C_i curve. If C_i<DP then I(C_i<DP) equals 1, else I(C_i<DP) equals 0. Please note that chloroplastic anaplerotic respiration is constant or zero above the deflection point and might thus contribute to R_x within this C_i range (Fig. 2a). To estimate both R_x (this paragraph) and R_a (below), we expanded the FvCB model describing RuBP-limited CO_2 assimilation by terms accounting for respiration and energy recycling by the anaplerotic pathway as

$$A_{\mathrm{j}} = \frac{(1 - \Gamma_*/C_{\mathrm{c}}) * (J + 4R_{\mathrm{a}}\mathrm{I}(C_{\mathrm{i}} < DP))}{4 + 8\,\Gamma_*/C_{\mathrm{c}}} - R_{\mathrm{a}}\mathrm{I}(C_{\mathrm{i}} < DP) - R_{\mathrm{x}} \qquad \text{[Eq. 2]}$$

where C_c is the CO_2 partial pressure in chloroplasts, Γ_* is the CO_2 compensation point in the absence of R_d, and J is the whole chain electron transport rate. Information on model building and parameterisation are given under Materials and Methods. Above the deflection point of the A/C_i curve, I(C_i<DP) equals 0, and RuBP-limited assimilation is given as

$$A_{\mathrm{j}} = \frac{(1 - \Gamma_*/C_{\mathrm{c}})J}{4 + 8\,\Gamma_*/C_{\mathrm{c}}} - R_{\mathrm{x}} \qquad \text{[Eq. 3]}$$

Varying R_x, we minimised the residual sum of squares between measured and modelled assimilation rates for values above the deflection point. The best fit was found at R_x=0.69 µmol CO_2 m^{-2} s^{-1} (Fig. 2b, red line, and Fig. 2c, black bars) corresponding to 5.6%, 4.8%, and 4% of net CO_2 assimilation at C_i=304, 516, and 1282 ppm, respectively (R_x/A*100). This is in good agreement with previously reported estimates (Atkin *et al.*, 2000; Teskey *et al.*, 2017) and thus corroborates the validity of model parameterisation including the chosen value for the maximal electron transport rate, J_{max}.

Process limiting CO_2 assimilation

Identifying processes limiting CO_2 assimilation is central in the field of plant breeding which, e.g., aims to increase plant productivity. In A/C_i curves, the initial linear increase below the deflection point is commonly attributed to Rubisco-limited assimilation. To test whether this interpretation holds for *Helianthus annuus* grown at low light, we modelled Rubisco-limited

assimilation, A_c, and compared modelling results with measurements of net CO_2 assimilation. In A_c models, the maximal rate of Rubisco carboxylation, V_{cmax}, is a crucial parameter (see Material and Methods). Close empirical relationships between J_{max} and V_{cmax} of the form $\ln(J_{max})=\beta_1+\beta_2*\ln(V_{cmax})$ where reported by Wullschleger (1993) (β_1=1.425, β_2=0.837, R^2=87.2, p<.001, n=110), Walker et al. (2014) using their own data (β_1=1.01, β_2=0.89, R^2=86.7, p<.001, n=301), and Walker et al. (2014) using data from a plant trait database (Kattge *et al.*, 2020) (β_1=1.668, β_2=0.75, R^2=78.9, p<.001, n=1048). Based on these relationships, we calculated V_{cmax} and modelled A_c (Fig. 2b, black lines). We found that $A_c >> A_j$ over the entire C_a range and A_j exceeds measured assimilation rates below the deflection point (Fig. 2b, red line vs. black dots). This indicates that in *Helianthus annuus* grown at low light, RuBP supply (=energy supply) limited net CO_2 assimilation over the entire C_a range. Rubisco-limitation and limitation by triose phosphate utilisation did not occur.

Integration of the anaplerotic pathway in carbon metabolism

Here, we assume that offsets between A_j and measured assimilation rates (Fig. 2b, red line vs. black dots) can be attributed to anaplerotic respiration in chloroplasts. This is supported by substantial increases in ε_{met} below DP reporting anaplerotic flux (Fig. 2a, dashed blue line, companion paper 2). Flux through the anaplerotic pathway, v_a, and anaplerotic respiration, R_a, are related as $v_a=R_a$ (Fig. 1). To estimate these rates in *Helianthus annuus* chloroplasts, we solved equation 2 for R_a as

$$v_a = R_a = \left(-\frac{(A_j + R_x) * (1 + 2\,\Gamma_*/C_c) - 0.25J * (1 - \Gamma_*/C_c)}{3\,\Gamma_*/C_c}\right) / \mathrm{I}(C_i < DP) \qquad \text{[Eq. 4]}$$

At C_i=136 and 202 ppm, we found anaplerotic flux rates of 2.99 and 2.39 µmol Ru5P m^{-2} s^{-1} (Fig. 2c, green bars) corresponding to 58.3 and 28.2% of net CO_2 assimilation (v_a/A*100, Fig. 3a), respectively. Furthermore, anaplerotic respiration governs total day respiration with contributions of 81.3 and 77.6% ($R_a/(R_a+R_x)$*100, Fig. 3b), respectively. Solving the basic assimilation model (von Caemmerer, 2000), $A=(1-\Gamma_*/C_c)v_c-R_d$, for v_c, and substituting R_d as in equation 1, we calculated rates of Rubisco carboxylation as

$$v_c = \frac{A_j + R_a \mathrm{I}(C_i < DP) + R_x}{1 - \Gamma_*/C_c} \qquad \text{[Eq. 5]}$$

At C_i=136 and 202 ppm, we found carboxylation rates of 13.49 and 15.11 µmol CO_2 m^{-2} s^{-1}, respectively (Fig 2c). Thus, anaplerotic flux/respiration rates correspond to 22.2 and 15.8% of Rubisco carboxylation (v_a/v_c*100, Fig. 3c), respectively. This represents percentages of futile carbon cycling involving CO_2 uptake by the CBC and liberation by the anaplerotic pathway (R_a/v_c*100). Rubisco oxygenation, v_o, was calculated by combining equations 2.16 and 2.18 from von Caemmerer (2000) as

$$v_o = 2\Gamma_*/C_c * v_c \qquad \text{[Eq. 6]}$$

At C_i=136 and 202 ppm, we found oxygenation rates of 9.36 and 7.13 µmol O_2 m^{-2} s^{-1}. Thus, oxygenation-to-carboxylation ratios amount to 0.69 and 0.47 (v_o/v_c), anaplerotic relative to photorespiratory CO_2 release amounts to 63.9 and 67% ($R_a/0.5v_o$*100, Fig. 3d), anaplerotic relative to total CO_2 release amounts to 25.7 and 36% ($R_a/(R_a+R_d+0.5v_o)$*100, Fig. 3e), and 13.1 and 10.7% of all RuBP is regenerated by the anaplerotic pathway ($v_a/(v_c+v_o)$*100, Fig. 3f), respectively.

Anaplerotic energy recycling

Offsets between measured net CO_2 assimilation rates and rates estimated by the FvCB model (RuBP-limited case) amount to 1.84 µmol CO_2 m^{-2} s^{-1} at C_i=136 ppm and 1.15 µmol CO_2 m^{-2} s^{-1} at C_i=202 ppm (Fig. 2b, black dots vs. red line). By contrast, anaplerotic respiration estimated by equation 4 amounts to 2.99 and 2.39 µmol CO_2 m^{-2} s^{-1}, respectively (Fig. 2c, green bars). Respective differences of 1.15 and 1.24 µmol CO_2 m^{-2} s^{-1} are explained by anaplerotic recovery of NADPH utilised to re-assimilate some of the respired CO_2 as follows (Fig. 2d, dark and light green bars). First fixation of anaplerotically respired CO_2 of 2.99 and 2.39 µmol CO_2 m^{-2} s^{-1} requires 10.13 and 7.04 µmol NADPH m^{-2} s^{-1}, respectively ($(2+2\Phi)R_a=(2+4\Gamma_*/C_c)R_a$). Associated anaplerotic flux recovers 5.98 and 4.78 µmol NADPH m^{-2} s^{-1} ($v_a'=2v_a$) enabling re-assimilation of 1.15 and 1.24 µmol CO_2 m^{-2} s^{-1} ($A_j=(C_c-\Gamma_*)J_a/(4C_c+8\Gamma_*)$, $J_a=2v_a'$), respectively. Thus, under RuBP-limiting conditions, anaplerotic flux decreases net CO_2 assimilation significantly but this decrease is fractionally offset by anaplerotic NADPH recovery. Consequently, anaplerotic respiration significantly exceeds the associated net carbon loss (58.3% vs. 35.8% of net CO_2 assimilation at C_i=136 ppm and 28.2% vs. 13.6% of net CO_2 assimilation at C_i=202 ppm). Below, we argue that anaplerotic flux may be upregulated under Rubisco-limited conditions as well. However, anaplerotic NADPH recovery can only support

fractional recovery of net CO_2 assimilation under RuBP-limiting conditions due to free catalytic capacity at Rubisco (cf. Eqs. 2, and 8).

Integration of the anaplerotic pathway in energy metabolism

In the FvCB modelling framework, NADPH and ATP demands of CO_2 assimilation are given as $(2+2\Phi)v_c=(2+4\Gamma_*/C_c)v_c$ and $(3+3.5\Phi)v_c=(3+7\Gamma_*/C_c)v_c$, respectively (von Caemmerer, 2000). This considers demands by RuBP regeneration and refixation of ammonia liberated in photorespiration. NADPH demands of anaplerotically respired CO_2 are reduced by $-2v_a$. Based on this, we calculated NADPH and ATP demands and corresponding ATP-to-NADPH ratios (Fig. 2e). Overall, we found increasing ATP-to-NADPH demand ratios (black circles) with decreasing C_i due to increasing ATP demands (purple triangles); NADPH demands remain constant (purple squares). Both photorespiration (black crosses, $(3+7\Gamma_*/C_c)/(2+4\Gamma_*/C_c)$) and anaplerotic flux (difference between black circles and crosses, $(3+7\Gamma_*/C_c)v_c/((2+4\Gamma_*/C_c)v_c-2v_a)$) exert significant effects. ATP-to-NADPH demand ratios by the CBC and photorespiration are 3/2=1.5 and 3.5/2=1.75, respectively. Linear electron transport is thought to produce insufficient ATP to satisfy these relative demands and other ATP producing processes such as cyclic electron flow are believed to be required (Joliot and Johnson, 2011). Thus, upregulation of the anaplerotic flux distinctly increases ATP requirements from these processes.

Anaplerotic effects on sucrose-to-starch carbon partitioning

Since the anaplerotic pathway branches off from the starch biosynthesis pathway (Fig. 1), anaplerotic flux changes may affect sucrose-to-starch carbon partitioning. To investigate this, we modelled sucrose-to-starch carbon partitioning as follows. Total carbon available to the sucrose and starch biosynthesis pathways is given as $v_c-0.5v_o-R_x$. All carbon entering the sucrose biosynthesis pathway is assumed to become sucrose. Carbon entering the starch biosynthesis pathway is either diverted anaplerotically into the CBC or becomes starch. For leaves of *Phaseolus vulgaris* grown at high C_i where anaplerotic flux can be expected to be downregulated, Sharkey et al. (1985) reported fluxes of ≈10 μmol C m^{-2} s^{-1} into sucrose and ≈15 μmol C m^{-2} s^{-1} into starch. Accordingly, we assumed a constant 2:3 carbon allocation ratio between the sucrose and starch biosynthesis pathways neglecting possible regulatory shifts at low C_i. Thus, we estimated sucrose-to-starch carbon partitioning ratios as

$$\frac{Sucrose}{Starch} = \frac{2/5\,(v_{\mathrm{c}} - 0.5v_{\mathrm{o}} - R_{\mathrm{x}})}{3/5\,(v_{\mathrm{c}} - 0.5v_{\mathrm{o}} - R_{\mathrm{x}}) - R_{\mathrm{a}}\mathrm{I}(C_{\mathrm{i}} < DP)} \qquad \text{[Eq. 7]}$$

For C_i≥304, =202, and =136 ppm, we found ratios of 0.67, 1.05, and 1.73, respectively (Fig. 2f, and Fig. 2c, dark vs. light blue bars). These findings indicate that the anaplerotic flux may be an important determinant of sucrose-to-starch carbon partitioning. Particularly, our model can explain increasing sucrose-to-starch carbon partitioning ratios with decreasing C_i as observed by Sharkey et al. (1985).

Discussion

Consistent evidence in support of anaplerotic flux in chloroplasts *in vivo*

Commonly, initial linear increases in A/C_i curves are interpreted in terms of Rubisco-limited net CO_2 assimilation (von Caemmerer, 2000). In accordance with recent isotope evidence (companion paper 2), we here explained it by the contribution of anaplerotic respiration to RuBP-limited assimilation.

Expanding FvCB photosynthesis models by terms accounting for anaplerotic respiration and energy recycling (Eqs. 2, and 8), we estimated anaplerotic flux rates and associated effects in leaf carbon and energy metabolism in *Helianthus annuus* based on gas exchange measurements. Below a change point, we found significant increases in anaplerotic flux with decreasing C_i (Fig. 2c). This is consistent with putative regulatory properties of the chloroplastic pathway detailed in the companion papers. Furthermore, while isotope and gas exchange analyses are methodologically independent, their results align well. At C_i=136, =202, and ≥304 ppm, anaplerotic flux corresponds to 58.3, 28.2, and 0% of net CO_2 assimilation, respectively (Fig. 3a). At the same time, metabolic deuterium fractionation at HC-1 of leaf starch, $\varepsilon_{\mathrm{met}}$, decreases significantly from 37 over -11 to -97‰, respectively (Fig. 2a). These consistencies corroborate that anaplerotic flux occurs in chloroplasts *in vivo*.

Anaplerotic flux in chloroplasts. A central component in carbon and energy metabolism

Anaplerotic flux has significant effects (*inter alia*) on net CO_2 assimilation, net carboxylation, net oxygenation (net photorespiration), day respiration, RuBP regeneration, NADPH supply, absolute ATP demands and ATP-to-NADPH demand ratios of photosynthesis, and possibly sucrose-to-starch carbon partitioning (Figs. 2, and 3). Thus, our work introduces the anaplerotic pathway as central component in carbon and energy metabolism of C_3 plants.

In *Helianthus annuus* at C_i=136 ppm, photorespiratory RuBP consumption distinctly exceeds the RuBP consumption by net CO_2 assimilation (Fig. 2c, 4.68*2=9.36 vs. 5.13 µmol RuBP m^{-2} s^{-1}). Thus, anaplerotic flux appears to be more important for maintaining photorespiration than net CO_2 assimilation. As detailed in the discussion of companion paper 2, maintaining photorespiration may be beneficial for nitrogen assimilation (Bloom, 2015). Assimilated nitrogen may be utilised to increase the photosynthetic capacity at the enzyme level resulting in increased plant source strength. Furthermore, maintenance and repair processes may require maintained nitrogen assimilation.

Anaplerotic flux under Rubisco-limited growth conditions

Here, we report evidence supporting anaplerotic flux in chloroplasts under RuBP-limited (=energy limited) conditions. However, several arguments suggest that anaplerotic flux may also occur under Rubisco-limited conditions. First, we reported isotope evidence for upregulated anaplerotic flux in *Pinus nigra* during periods of drought, i.e., low C_i (companion paper 1). These samples come from an open stand with low above-ground competition among trees. During dry growing seasons with upregulated anaplerotic flux, average energy inputs into the system were significantly higher than in other years (global radiation=3772 vs. 3619 MJ m^{-2}; one-tailed t-test preceded by equal variance test: p=0.25, n=9 and 19; data source: see companion paper 1, radiation timeseries starts in 1964). Thus, these trees likely received sufficient energy inputs, especially during dry years, and photosynthesis was likely not RuBP but Rubisco limited. Second, anaplerotic flux is upregulated under low C_i proposedly via decreasing concentrations of 3-phosphoglycerate and erythrose 4-phosphate in chloroplasts (see companion papers). Low C_i and high light frequently co-occur in plant ecosystems. This would promote low concentrations of 3-phosphoglycerate and erythrose 4-phosphate (due to low C_i) and Rubisco-limited conditions (due to high energy input). That is, regulatory prerequisites for anaplerotic flux may be met. Third, upregulation of anaplerotic flux proposedly occurs under source-limiting conditions (companion papers). These can occur under RuBP as well as Rubisco-limited conditions.

Anaplerotic flux into the CBC: Implications for models and estimations

Anaplerotic respiration liberates CO_2 derived from the C-1 carbon of plastidial G6P. Hence, the carbon isotope composition of this CO_2 can be expected to depend on fractionation effects of enzymes modifying G6P C-1 atom bonds, namely phosphoglucose isomerase, PGI, and

glucose-6-phosphate dehydrogenase, G6PD (companion paper 2). Gilbert et al. (2012) measured *in vitro* isotope effects of microbial glucose isomerase and argued plant PGI will have similar effects since it operates by the same reaction mechanism. For glucose C-1, these authors reported kinetic and equilibrium $^{12}C/^{13}C$ effects of ≈1.004 and ≈0.987, respectively. Upregulations of the anaplerotic flux are associated with shifts towards PGI equilibrium (see companion papers). Thus, G6P may become increasingly ^{13}C-1 enriched with increasing anaplerotic flux (Wieloch *et al.*, 2018). This ^{13}C-1 enriched G6P serves as anaplerotic substrate and in the absence of other fractionations would result in the release of ^{13}C enriched CO_2. However, G6PD catalyses the first and committed step of the anaplerotic pathway with an *in vitro* kinetic $^{12}C/^{13}C$ effect of ≈1.0165 at 6-phosphogluconolactone C-1 (Hermes *et al.*, 1982). *In vivo*, this effect should cause further G6P ^{13}C-1 enrichment but ^{13}C depletion of respired CO_2. Depending on whether fractionation effects by PGI or G6PD prevail *in vivo*, anaplerotically respired CO_2 will be ^{13}C enriched and carbon remaining in the metabolic network will be ^{13}C depleted or *vice versa*. In current $\delta^{13}C$ models, anaplerotic fractionation and its C_i dependency is not detailed. Thus, estimates of C_i/C_a, water-use efficiency, and mesophyll conductance based on these models may be biased.

Besides carbon and hydrogen isotope effects, anaplerotic flux has significant effects (*inter alia*) on day respiration, and net CO_2 assimilation (Figs. 2, and 3). Neglecting these effects in models of isotope composition, physiological quantities, and plant growth can potentially lead to biased analytical results with increasing errors towards lower C_i levels. For instance, relationships between mesophyll conductance and C_i or irradiation as well as underlying mechanisms have remained enigmatic despite significant research efforts (Gu and Sun, 2014). Considering anaplerotic flux may improve assessments of mesophyll conductance and other physiological and isotopic quantities as well as plant growth.

Outlook

Anaplerotic flux affects plant carbon and energy metabolism and balances significantly (Figs. 2, and 3). Thus, it requires comprehensive characterisation including impacts on plant functioning, biomass production, the global carbon cycle, and climate change. Photosynthesis modelling tools introduced here may enable flux analyses across scales.

While we believe that our dataset is sufficiently large to distinguish two commonly observed phases in A/C_i curves, similar investigations with larger datasets are needed. These may enable

(i) elucidation of the precise (possibly non-linear) relationship between v_a and C_i and, (ii) its incorporation into photosynthesis models.

Material and Methods

Samples

Helianthus annuus L. cv. Zebulon samples are described in companion paper 2.

Leaf gas exchange measurements

Gas exchange measurements were performed with a two-channel fast-response system described previously (Laisk and Edwards, 1997). A sandwich-type round chamber enclosed a leaf area of 8.04 cm^2. Gas flow was maintained at 0.5 mmol s^{-1}. Measurements were performed at CO_2 concentrations similar to those applied in the growth chamber over two days (C_a=173 ± 0.1SE, 269 ± 0.1SE, 433 ± 0.1SE, 675 ± 0.2SE, 1431 ± 0.4SE ppm). To maintain temperatures of 22 ± 0.5 °C, the upper leaf side was attached to a thermostated glass window by starch gel. Light was provided by a Schott KL 1500 lamp (Walz Heinz GmbH, Effeltrich, Germany) and measured by a LI-185 quantum sensor (LiCor, Lincoln, USA). Measurements were performed at 300 µmol photons m^{-2} s^{-1} yielding C_i=136 ± 1SE, 202 ± 4SE, 304 ± 8SE, 516 ± 14SE, 1282 ± 16SE ppm.

Models of net CO_2 assimilation that consider the anaplerotic pathway

RuBP-limited CO_2 assimilation ultimately results from limitations in incoming electrons required by the CBC and photorespiration in the forms of NADPH and ATP (von Caemmerer, 2000). Commonly, it is assumed that NADPH rather than ATP synthesis via whole chain electron transport is limiting. Combined NADPH requirements by the CBC and photorespiration are given as $(2+2\Phi)v_c$ where Φ is the ratio of the oxygenation-to-carboxylation rate of Rubisco, v_o and v_c , respectively (Farquhar and von Caemmerer, 1982). Since synthesis of 1 mol NADPH requires 2 mol electrons, the corresponding energy requirement is given as $(4+4\Phi)v_c$ (von Caemmerer, 2000). Per 1 mol CO_2 respired by the anaplerotic pathway, 2 mol NADPH (4 mol electrons) are recycled, i.e., can be reused by the CBC and photorespiration (Fig. 1). Hence, NADPH and electron recycling rates by the anaplerotic pathway are given as $2R_a\mathrm{I}(C_i<\mathrm{DP})$ and $J_a\mathrm{I}(C_i<\mathrm{DP})=4R_a\mathrm{I}(C_i<\mathrm{DP})$, respectively. Then, energy available to the CBC and photorespiration equals the incoming energy, J, plus energy recycled by the anaplerotic pathway as $J+J_a\mathrm{I}(C_i<\mathrm{DP})=J+4R_a\mathrm{I}(C_i<\mathrm{DP})$. This energy amount can support energy requirements of the CBC and photorespiration as $J+4R_a\mathrm{I}(C_i<\mathrm{DP})=(4+4\Phi)v_c$. Solving for v_c

gives v_c=(J+4R_aI(C_i<DP))/(4+4Φ). In the basic FvCB model, net CO_2 assimilation is expressed as A=(1-0.5Φ)v_c-R_d (von Caemmerer, 2000). Since Φ=2Γ_*/C_c (von Caemmerer, 2000), equations can be rewritten as v_c=(J+4R_aI(C_i<DP))/(4+8Γ_*/C_c) and A=(1-Γ_*/C_c)v_c-R_d. Substituting R_d (Eq. 1) and v_c in the latter equation gives the RuBP-limited net CO_2 assimilation that considers the anaplerotic pathway as

$$A_\mathrm{j} = \frac{(1-\Gamma_*/C_\mathrm{c}) * (J + 4R_\mathrm{a}\mathrm{I}(C_\mathrm{i} < DP))}{4 + 8\,\Gamma_*/C_\mathrm{c}} - R_\mathrm{a}\mathrm{I}(C_\mathrm{i} < DP) - R_\mathrm{x} \qquad \text{[Eq. 2]}$$

In the FvCB modelling framework, Rubisco-limited CO_2 assimilation is given as A_c=V_{cmax}(C_c-Γ_*)/(C_c+K_c(1+O/K_o))-R_d where V_{cmax} is the maximal rate of Rubisco carboxylation, O is oxygen partial pressure, and K_c and K_o are the Michaelis-Menten constants of Rubisco carboxylation and oxygenation, respectively (von Caemmerer, 2000). Implementing the anaplerotic pathway into this model requires substitution of R_d as in equation 1 as

$$A_\mathrm{c} = \frac{V_\mathrm{cmax}(C_\mathrm{c} - \Gamma_*)}{C_\mathrm{c} + K_\mathrm{c}(1 + O/K_\mathrm{o})} - R_\mathrm{a}\mathrm{I}(C_\mathrm{i} < DP) - R_\mathrm{x} \qquad \text{[Eq. 8]}$$

Parameterisation of models of net CO_2 assimilation

C_c was calculated according to Fick's first law as C_c=C_i-A/g_m. Schäufele et al. (2011) grew *Helianthus annuus* under conditions similar to those applied here (20 °C, 600 µmol photons m^{-2} s^{-1}). These authors estimated a g_m value of 0.45 mol CO_2 m^{-2} s^{-1} which we used to calculate C_c. Kinetic constants of Rubisco are highly conserved among C_3 species (von Caemmerer, 2000). To obtain robust estimates, we calculated arithmetic means of reported *in vitro* measurements of K_c, K_o, and the ratio of maximal rates of oxygenation to carboxylation, V_{omax}/V_{cmax} using data listed in von Caemmerer (2000) from *Spinacia oleracea*, *Glycine max*, and *Nicotiana tabacum*. K_c and K_o were corrected for leaf temperature (21.8 °C) using published Q_{10} values (von Caemmerer, 2000) which gave K_c=260 ± 24SE µbar, and K_o=282 ± 9SE mbar. A temperature correction was not required for the V_{omax}/V_{cmax} ratio since V_{omax} and V_{cmax} exhibit the same Q_{10} (von Caemmerer, 2000). Thus, we used V_{omax}/V_{cmax}=0.48 ± 0.06SE mbar. O was calculated from gas exchange measurement read-outs of dissolved oxygen concentrations which gave O=206781 µbar. For R_d, we used our own estimate of R_x=0.69 µmol CO_2 m^{-2} s^{-1} (see main text). We calculated Rubisco relative specificity, $S_{o/c}$, and Γ_* as

$S_{o/c}=1/(V_{omax}/V_{cmax})*K_o/K_c=2359 \pm 43SE$ [bar/bar] and $\Gamma_*=0.5O/S_{o/c}=43.8 \pm 0.8SE$ μbar. Electron transport rate is given as $J=(I_2+J_{max}-SQRT((I_2+J_{max})^2-4\theta I_2 J_{max}))/2\theta$ where θ is an empirical curvature factor commonly set to 0.7 (von Caemmerer, 2000). Useful light absorbed by photosystem II is given as $I_2=I*abs(1-f)/2$ where I is incident irradiance, abs is the absorptance of leaves commonly set to 0.85 (von Caemmerer, 2000), and f is a correction factor for the spectral quality of light commonly set to 0.15 (von Caemmerer, 2000). A measured value of I=258 μmol m^{-2} s^{-1} was used. From data listed in Wullschleger (1993), we calculated the average J_{max} for *Helianthus annuus* and corrected it for temperature using the Q_{10} listed in von Caemmerer (2000) which gave J_{max}=216 μmol m^{-2} s^{-1}. The data point contributed by Siebke et al. (1990) was identified as outlier and excluded.

Acknowledgements

We thank Jun Yu (Umeå University) for helpful discussions.

Author contributions

T.W. conceived the study and led the research. A.A., and J.S. prepared samples and acquired gas exchange data. T.W. expanded FvCB models. T.W. analysed the data. T.W. wrote the paper with input from A.A.

Competing interests: The authors declare no competing interests.

References

Atkin OK, Millar AH, Gardeström P, Day DA. 2000. Photosynthesis, carbohydrate metabolism and respiration in leaves of higher plants. In: Leegood RC, Sharkey TD, von Caemmerer S, eds. Photosynthesis: Physiology and Metabolism. Dordrecht: Springer Netherlands, 153–175.

Bloom AJ. 2015. Photorespiration and nitrate assimilation: A major intersection between plant carbon and nitrogen. Photosynthesis Research **123**, 117–128.

von Caemmerer S. 2000. *Biochemical models of leaf photosynthesis*. CSIRO. http://photosynthesis.org.au/wp-content/uploads/2017/09/von-Caemmerer-2000-Biochem.Models.pdf. Accessed: 1 August 2021.

Eicks M, Maurino V, Knappe S, Flügge U-I, Fischer K. 2002. The plastidic pentose phosphate translocator represents a link between the cytosolic and the plastidic pentose phosphate pathways in plants. Plant Physiology **128**, 512–522.

Farquhar GD, Caemmerer S, Berry JA. 1980. A biochemical model of photosynthetic CO_2 assimilation in leaves of C_3 species. Planta **149**, 78–90.

Farquhar GD, von Caemmerer S. 1982. Modelling of photosynthetic response to environmental conditions. In: Lange OL, Nobel PS, Osmond CB, Ziegler H, eds. Physiological plant ecology II: Water relations and carbon assimilation. Berlin, Heidelberg: Springer Berlin Heidelberg, 549–587.

Gilbert A, Robins RJ, Remaud GS, Tcherkez G. 2012. Intramolecular ^{13}C pattern in hexoses from autotrophic and heterotrophic C_3 plant tissues. Proceedings of the National Academy of Sciences of the United States of America **109**, 18204–18209.

Gu L, Sun Y. 2014. Artefactual responses of mesophyll conductance to CO_2 and irradiance estimated with the variable *J* and online isotope discrimination methods. Plant, Cell & Environment **37**, 1231–1249.

Hermes JD, Roeske CA, O'Leary MH, Cleland WW. 1982. Use of multiple isotope effects to determine enzyme mechanisms and intrinsic isotope effects. Malic enzyme and glucose 6-phosphate dehydrogenase. Biochemistry **21**, 5106–5114.

Joliot P, Johnson GN. 2011. Regulation of cyclic and linear electron flow in higher plants. Proceedings of the National Academy of Sciences of the United States of America **108**, 13317–13322.

Kattge J, Bönisch G, Díaz S, Lavorel S, Prentice IC, Leadley P, Tautenhahn S, Werner GD, Aakala T, Abedi M. 2020. TRY plant trait database–enhanced coverage and open access. Global Change Biology **26**, 119–188.

Laisk A, Edwards GE. 1997. CO_2 and temperature-dependent induction in C_4 photosynthesis: an approach to the hierarchy of rate-limiting processes. Functional Plant Biology **24**, 505–516.

Schäufele R, Santrucek J, Schnyder H. 2011. Dynamic changes of canopy-scale mesophyll conductance to CO_2 diffusion of sunflower as affected by CO_2 concentration and abscisic acid. Plant, Cell & Environment **34**, 127–136.

Sharkey TD. 1985. Photosynthesis in intact leaves of C_3 plants: Physics, physiology and rate limitations. The Botanical Review **51**, 53–105.

Sharkey TD, Berry JA, Raschke K. 1985. Starch and sucrose synthesis in *Phaseolus vulgaris* as affected by light, CO_2, and abscisic acid. Plant Physiology **77**, 617–620.

Sharkey TD, Preiser AL, Weraduwage SM, Gog L. 2020. Source of ^{12}C in Calvin-Benson cycle intermediates and isoprene emitted from plant leaves fed with $^{13}CO_2$. The Biochemical Journal **477**, 3237–3252.

Sharkey TD, Weise SE. 2016. The glucose 6-phosphate shunt around the Calvin–Benson cycle. Journal of Experimental Botany **67**, 4067–4077.

Siebke K, Laisk A, Oja V, Kiirats O, Raschke K, Heber U. 1990. Control of photosynthesis in leaves as revealed by rapid gas exchange and measurements of the assimilatory force FA. Planta **182**, 513–522.

Teskey RO, McGuire MA, Bloemen J, Aubrey DP, Steppe K. 2017. Respiration and CO_2 fluxes in trees. In: Tcherkez G, Ghashghaie J, Sharkey TD, eds. Advances in Photosynthesis and Respiration. Plant respiration: Metabolic fluxes and carbon balance. Cham: Springer International Publishing, 181–207.

Walker AP, Beckerman AP, Gu L, Kattge J, Cernusak LA, Domingues TF, Scales JC, Wohlfahrt G, Wullschleger SD, Woodward FI. 2014. The relationship of leaf photosynthetic traits - V_{cmax} and J_{max} - to leaf nitrogen, leaf phosphorus, and specific leaf area: a meta-analysis and modeling study. Ecology and evolution **4**, 3218–3235.

Wieloch T, Ehlers I, Yu J, Frank D, Grabner M, Gessler A, Schleucher J. 2018. Intramolecular ^{13}C analysis of tree rings provides multiple plant ecophysiology signals covering decades. Scientific Reports **8**, 5048.

Wullschleger SD. 1993. Biochemical limitations to carbon assimilation in C_3 plants. A retrospective analysis of the A/C_i curves from 109 Species. Journal of Experimental Botany **44**, 907–920.